System-Orthogonal Functions for Sound Speed Profile Perturbation

Wen Xu, *Senior Member, IEEE,* and Henrik Schmidt

***Abstract*—Empirical orthogonal functions (EOFs) are typically derived from direct measurements of the sound speed profile (SSP) and they are orthogonal in regard to the statistics of the SSP uncertainty. Viewed from the output end of a particular sonar system, however, the effect of an error in one EOF is usually coupled with the effect of the error in another due to the strongly nonlinear relation between the SSP parameters and the system response. In this paper, a new set of basis functions, orthogonal in regard to sonar performance measure, is developed to characterize SSP perturbations. The performance measure used is the Cramer–Rao bound (CRB) for SSP expansion coefficients derived from a full-field random Gaussian signal model; a closed-form, analytical solution is obtained for both the range-independent and adiabatically range-dependent environments. The derived functions make the CRB matrix diagonal, decoupling the errors in the estimation of the expansion coefficients. Compared to the EOFs, the new set of basis functions depends on both the statistics of the sound speed uncertainty and the sound waveguide propagation property; it incorporates the measurement noise as well. The development makes possible the investigation of the relative significance of the individual basis functions in system response; it also provides a novel framework for optimum acoustic parameterization in adaptive rapid environmental assessment.**

***Index Terms*—Cramer–Rao bound (CRB), empirical orthogonal functions (EOFs), matched-field methods, optimum acoustic parameterization, system-orthogonal functions.**

I. Introduction

UNCERTAINTY of the acoustic environment is one of the major obstacles to adapting new model-based sonar processing frameworks, such as matched-field processing (MFP), to the coastal environment [1]–[3]. It propagates through the complete chain for sonar performance: Environment, acoustics, processing, and operator. Recently a general approach of acoustic data assimilation has been developed [4], aiming to reducing such uncertainty by assimilating instant environmental measurements to dynamical oceanographic models. To achieve that in a real application, one needs to identify the most significant environment parameters observable in system response, and design an optimal deployment of the available resources to make direct measurements on those parameters. This would constitute the kernel of adaptive rapid environmental assessment.

To limit the degrees of freedom ocean parameters are often represented in terms of empirical orthogonal functions (EOFs). In the water column, the EOFs are derived from direct measurements of sound speed profile (SSP) and they are orthogonal in regard to the statistics of the SSP variations [5]. Viewed from the sonar output end, however, the effect of an error in one EOF is usually coupled with the effect of the error in another, attributed to the strongly nonlinear relation between the SSP parameters and the response of a particular sonar system (cf., e.g., discussions on modal phase perturbation in [3]). Thus, the relative significance of the individual EOFs cannot be directly determined.

In this paper, we derive a new set of basis functions uncoupled in system response. Specifically, we represent the SSP variations in terms of an arbitrary set of basis functions, and treat the individual coefficients as random parameters estimated alone or together with the unknown source location parameter using matched-field methods. We then evaluate the Cramer–Rao bound (CRB) [6], [7] for the chosen parameters and determine a set of basis functions so that the CRB matrix corresponding to those SSP coefficients is diagonal. In this way, errors in the estimation of individual coefficients are decoupled. The coastal environment has variability over a wide range of spatial scales; similar to the EOFs, the new parameterization is in the form of distribution functions directly representing the different scales of such variability.

The concept of the optimal orthogonal function has been introduced in the context of ocean acoustic tomography for linear travel-time inversion of sound speed [8]. Expressing the estimation error explicitly in terms of arbitrary basis functions, the optimal ones are solved by minimizing the error. This optimal parameterization takes into account both the prior information on SSP variations and the resolution with which each variation can be measured by a particular system configuration. Some preliminary results show more accurate tomographic inversions than are possible with the EOFs.

The rest of the paper is organized as follows. The acoustic propagation modeling under random sound speed perturbation is first introduced in Section II. Section III then presents the Fisher information matrix (FIM) associated with the matched-field source localization/environmental parameter estimation. Section IV derives such matrix for SSP expansion coefficients for both range-independent and adiabatically range-dependent cases and solves the new basis functions accordingly. Section V presents some examples, and some future issues on simultaneous source location and SSP coefficient estimation are discussed in Section VI. Finally, Section VII concludes the paper.

Manuscript received July 18, 2003; accepted October 13, 2005. This work was supported by the Office of Naval Research under Grant N00014-01-1-0817. **Associate Editor: R. Spindel.**

W. Xu was with the Department of Ocean Engineering, Massachusetts Institute of Technology, Cambridge, MA 02139 USA. He is now with the Teledyne RD Instruments, San Diego, CA 92131 USA (e-mail: wenx@ieee.org).

H. Schmidt is with the Department of Mechanical Engineering, Massachusetts Institute of Technology, Cambridge, MA 02139 USA (e-mail: henrik@keel.mit.edu).

Digital Object Identifier 10.1109/JOE.2006.872221

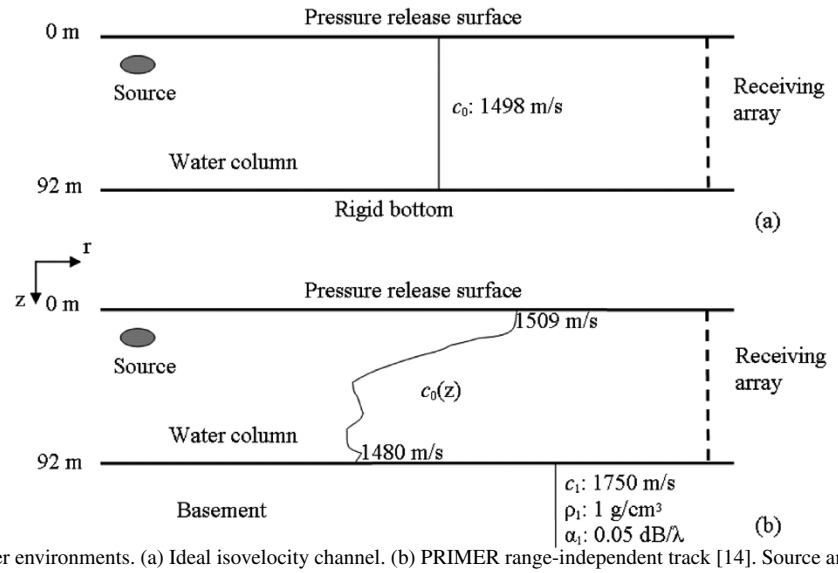

Fig. 1. Example shallow water environments. (a) Ideal isovelocity channel. (b) PRIMER range-independent track [14]. Source and receiver configuration is also shown.

II. Acoustic Propagation Modeling With Random Sound Speed Perturbation

Matched-field methods concern estimation of source locations and/or ocean environmental parameters by exploiting full wave modeling of acoustic waveguide propagation. They are particularly useful for the case of large vertical aperture or very long horizontal array with some tilt where nonplane wave signals are encountered. Consider a stratified waveguide model for the seismo/acoustic environment, which consists of water column, multilayer sediment and semi-infinite basement, and can be either range-dependent or independent (see Fig. 1 for an example). A point source radiates narrowband or broadband signals, and the signal field is sampled by a vertical receiving array. The waveguide transfer function from the source to the receiver is the unit point source solution to the wave equation (Green's function) [9], which is a function of the source-receiver configuration as well as environmental parameters.

The SSP in the water column is one of the most important parameters in determining the sound waveguide propagation, for example, the existence of duct propagation or the fraction of energy down to the bottom. It is, however, difficult to treat this as deterministic due to both its temporal and spatial variations. In the following, we present wave field solutions under random SSP perturbations based on the results in [3]. The results are detailed in the context of range-dependent perturbations; the range-independent problem is then solved as a special case.

A. SSP Orthogonal Function Representation

The SSP in a range-dependent environment can be described by a mean profile, $c_0(z)(z$: depth), plus some zero-mean random perturbations, $\Delta c(r,z)(r$: range). $\Delta c(r,z)$ is often expressed in terms of a set of orthogonal functions, $\{\psi_l(z)\}$,[1] so that

$$\Delta c(r,z) = \sum_{l=1}^{L} w_l(r)\psi_l(z) \tag{1}$$

[1]An alternative and probably more realistic representation uses two-dimensional (2-D) basis functions in r and z, which we would leave as future effort.

with $w_l(r)$ as random coefficients. In reality, the SSP and its variation are denoted by, i.e., N_Z, discrete depth points, leading to a vector form representation

$$\Delta\mathbf{c}(r) = \mathbf{\Psi}\mathbf{w}(r) \tag{2}$$

where

$$\Delta\mathbf{c}(r) = [\Delta c(r,Z_1) \quad \Delta c(r,Z_2) \quad \dots \quad \Delta c(r,Z_{N_Z})]^T \tag{3}$$

$$\mathbf{w}(r) = [w_1(r) \quad \dots \quad w_l(r) \quad \dots \quad w_L(r)]^T \tag{4}$$

$$\mathbf{\Psi} = [\boldsymbol{\psi}_1 \quad \dots \quad \boldsymbol{\psi}_l \quad \dots \quad \boldsymbol{\psi}_L] \tag{5}$$

$$\boldsymbol{\psi}_l = [\psi_l(Z_1) \quad \psi_l(Z_2) \quad \dots \quad \psi_l(Z_{N_Z})]^T \tag{6}$$

and $[]^T$ denotes the matrix transpose operation. Note that when $L = N_Z$, $\mathbf{\Psi}$ is an orthonormal set with $\mathbf{\Psi}\mathbf{\Psi}^T = \mathbf{\Psi}^T\mathbf{\Psi} = \mathbf{I}$, where $\mathbf{I}$ is an identity matrix with a dimension defined in the context.

The complete EOF set is an example orthonormal basis, which contains all the eigenvectors of the covariance matrix of the random speed perturbations [5]. Denote the range-averaged SSP perturbation by $\Delta\bar{\mathbf{c}} = \mathrm{E}_r[\Delta\mathbf{c}(r)]$ and the associated covariance matrix by $\mathbf{K}_{\Delta\bar{\mathbf{c}}} = \mathrm{E}_{\Delta\bar{\mathbf{c}}}[\Delta\bar{\mathbf{c}}\,\Delta\bar{\mathbf{c}}^T]$, then

$$\mathbf{K}_{\Delta\bar{\mathbf{c}}}\mathbf{\Psi}_{\mathrm{EOF}} = \mathbf{\Psi}_{\mathrm{EOF}}\mathbf{\Lambda}_{\mathrm{EOF}} \tag{7}$$

where $\mathbf{\Lambda}_{\mathrm{EOF}}$ is the diagonal eigenvalue matrix. The covariance matrix is usually estimated from the onsite and/or historical SSP measurements. Each eigenvector represents one mode of the SSP variation along depth while the corresponding eigenvalue indicates the amount of energy in that mode. Often, due to the correlation in SSP data, those eigenvalues diminish rapidly so that only a few eigenvectors dominate the SSP characterization; thus, the size of the EOF representation can be significantly reduced ($L << N_Z$).

Obviously an arbitrary orthogonal basis can be related to the EOF basis through a unitary transform

$$\mathbf{\Psi} = \mathbf{\Psi}_{\mathrm{EOF}}\mathbf{E} \tag{8}$$

where $\mathbf{E}\mathbf{E}^T = \mathbf{E}^T\mathbf{E} = \mathbf{I}$. This allows a size-reduced (orthogonal but not orthonormal) basis representation based on the size-reduced EOFs. In that case, the unitary transform matrix,

$\mathbf{E}$, has a dimension of the number of retained EOFs. When $\mathbf{E}$ is an identity matrix, the result reduces to that of EOFs. Using (8), (2) becomes

$$\Delta\mathbf{c}(r) = \mathbf{\Psi}_{\mathrm{EOF}}\mathbf{E}\mathbf{w}(r). \tag{9}$$

B. Pressure Field Under a Perturbed Environment

The pressure field in the case of $\Delta c(r,z) << c_0(z)$ has been derived based on the adiabatic modal phase approximation [3]. Assume that a vertical receiving array is deployed at $r = 0$, consisting of M sensors uniformly located from z_1 to z_M with spacing Δd, and a point source of frequency f is located at range r_s and depth z_s. The Green's function can be expressed as a sum of normal modes [3]

$$g(z_m; r_s, z_s) = \sqrt{2\pi}\sum_{n=1}^{N}\frac{\varphi_n^{(0)}(z_m)\varphi_n^{(0)}(z_s)}{\sqrt{k_n^{(0)}r_s}} \times e^{jk_n^{(0)}r_s - \delta_n^{(0)}r_s}e^{j\int_0^{r_s}\Delta k_n(r)\,dr}, \quad m = 1,\ldots,M \tag{10}$$

where $k_n^{(0)}, n = 1,\ldots,N$, are modal horizontal wave numbers; $\delta_n^{(0)}, n = 1,\ldots,N$, are modal attenuations; $\varphi_n^{(0)}(z), n = 1,\ldots,N$ are modal shape functions; N is the number of the propagation modes; and the superscript$^{(0)}$ indicates the association with the mean profile. The wave number perturbation, $\Delta k_n(r)$, is attributed to the SSP perturbation; it then affects the Green's function through an added modal phase variation.

Some closed-form solution of the wave number perturbation has been developed for small SSP perturbations by applying the perturbation theory to wave equation [3], [10]. Note that $\Delta c(r,z)$ is nonzero only for $z = 0$ to z_{B} (z_{B} is the bottom depth); hence, the perturbation in modal horizontal wave number under the current configuration is derived as

$$\begin{aligned}\Delta k_n(r) &= \frac{-1}{k_n^{(0)}}\int_0^{z_B}\frac{\left|\varphi_n^{(0)}(z)\right|^2 k^{(0)}(z)^2}{c_0(z)}\Delta c(r,z)\,dz \\ &= \frac{-1}{k_n^{(0)}}\int_0^{z_B}\frac{\left|\varphi_n^{(0)}(z)\right|^2 k^{(0)}(z)^2}{c_0(z)}\sum_{l=1}^{L}w_l(r)\psi_l(z)\,dz \\ &= \sum_{l=1}^{L}w_l(r)\int_0^{z_B}\frac{-\left|\varphi_n^{(0)}(z)\right|^2 k^{(0)}(z)^2}{k_n^{(0)}c_0(z)}\psi_l(z)\,dz\end{aligned} \tag{11}$$

where $k^{(0)}(z) = 2\pi f/c_0(z)$ is the wave number for the mean profile and (1) is used for the second equality.

Obviously, $\Delta k_n(r)$ in (11) is a real number. Substituting (11) into (10), the added phase term contains the following range integration:

$$\bar{w}_l(r_s) = \int_0^{r_s} w_l(r)\,dr. \tag{12}$$

It is this averaged SSP coefficient term that is involved in perturbed sound propagation. An interesting observation from (12) is that when the coherent range of the random sound perturbation is much less than the source range, $\bar{w}_l(r_s)$ is subject to a Gaussian distribution due to the central limit theorem regardless of the distribution of individual $w_l(r)$ [3].

To evaluate (11), the integration of continuous variable needs to be transformed to a sum of discrete points. The number of discrete depth points is normally chosen such that both individual $\psi_l(z)$ and $\varphi_n^{(0)}(z)$ are well sampled because $c_0(z)$ and then $k^{(0)}(z)$ are normally far less oscillatory. Typical sampling grid for $\{\psi_l(z)\}$ works for $\{\varphi_n^{(0)}(z)\}$ as well, particularly for the low-order propagation modes in shallow water. In the case that $\{\varphi_n^{(0)}(z)\}$ shows more oscillations, the integration step size is determined from $\{\varphi_n^{(0)}(z)\}$ and the derivations below can still be followed with the SSP interpolated accordingly.

From now on, we assume (11) can be evaluated in terms of samples at the same N_Z depth points as in (3). Denote (13)–(15), shown at the bottom of the page, with $\Delta z = (z_B)/(N_Z - 1)$. The added phase perturbation for N individual modes is then expressed by

$$\begin{aligned}\Delta\mathbf{\Theta}(r_s) &= [\Delta\Theta_1(r_s) \quad \ldots \quad \Delta\Theta_N(r_s)]^T \\ &= \mathbf{F}^T\mathbf{\Psi}_{\mathrm{EOF}}\mathbf{E}\bar{\mathbf{w}}(r_s)\end{aligned} \tag{16}$$

where the integration in (11) is approximated by the matrix product. A vector form of the Green's function is stated by

$$\mathbf{g}(r_s, z_s, \bar{\mathbf{w}}) = \mathbf{U}_0\mathbf{S}_0(r_s, z_s)\mathbf{p} \tag{17}$$

where (18)–(20), shown at the bottom of the next page, and $\mathbf{p}$ is a vector of element-wise exponential

$$\mathbf{p} = e^{j\Delta\mathbf{\Theta}} = [e^{j\Delta\Theta_1} \quad e^{j\Delta\Theta_2} \quad \ldots \quad e^{j\Delta\Theta_N}]^T. \tag{21}$$

Note that $\bar{\mathbf{w}}$ is the unknown (random) environmental parameter set.

C. Special Case: Range-Independent SSP Perturbation

For a range-independent environment, we have for the SSP perturbation

$$\Delta c(z) = \sum_{l=1}^{L} w_l\psi_l(z). \tag{22}$$

$$\bar{\mathbf{w}}(r_s) = [\bar{w}_1(r_s) \quad \ldots \quad \bar{w}_l(r_s) \quad \ldots \quad \bar{w}_L(r_s)]^T \tag{13}$$

$$\mathbf{f}_n = \left[\frac{-\left|\varphi_n^{(0)}(Z_1)\right|^2 k^{(0)}(Z_1)^2}{k_n^{(0)}c_0(Z_1)}\frac{\Delta z}{2} \quad \ldots \quad \frac{-\left|\varphi_n^{(0)}(Z_i)\right|^2 k^{(0)}(Z_i)^2}{k_n^{(0)}c_0(Z_i)}\Delta z \quad \ldots \quad \frac{-\left|\varphi_n^{(0)}(Z_{N_Z})\right|^2 k^{(0)}(Z_{N_Z})^2}{k_n^{(0)}c_0(Z_{N_Z})}\frac{\Delta z}{2}\right]^T \tag{14}$$

$$\mathbf{F} = [\mathbf{f}_1 \quad \ldots \quad \mathbf{f}_n \quad \ldots \quad \mathbf{f}_N] \tag{15}$$

The SSP coefficients are no longer a function of range and the integration in (12) becomes $w_l r_s$. Denote

$$\mathbf{w} = [w_1 \quad \dots \quad w_l \quad \dots \quad w_L]^T. \tag{23}$$

The Green's function is again given by (17) with a modified phase perturbation

$$\Delta\boldsymbol{\Theta} = \mathbf{F}^T \boldsymbol{\Psi}_{\mathrm{EOF}} \mathbf{E} \mathbf{w} r_s. \tag{24}$$

Note that $\boldsymbol{\Psi}_{\mathrm{EOF}}$ is now derived from $\mathbf{K}_{\boldsymbol{\Delta c}} = \mathrm{E}_{\Delta \mathbf{c}}[\Delta \mathbf{c} \Delta \mathbf{c}^T]$.

III. Cramer–Rao Bound on Matched-Field Methods

The development in this paper focuses on operation of matched-field methods in the high signal-to-noise ratio (SNR) region. In this region, the maximum likelihood estimator (MLE) achieves the Cramer–Rao lower bound [6], thus making its performance analysis analytically tractable.

A. Local, Bayesian, and Hybrid Cramer–Rao Bound

The CRB states for the mean-square error matrix

$$\boldsymbol{\Sigma} = \mathrm{E}_{\hat{\boldsymbol{\theta}}, \boldsymbol{\theta}}[(\hat{\boldsymbol{\theta}} - \boldsymbol{\theta})(\hat{\boldsymbol{\theta}} - \boldsymbol{\theta})^T] \geq \mathbf{J}^{-1} \tag{25}$$

where $\boldsymbol{\theta}$ is the parameter vector to be estimated; $\hat{\boldsymbol{\theta}}$ denotes the estimate of $\boldsymbol{\theta}$; and $\mathbf{J}$ is the Fisher information matrix (FIM) [6]. In the case that the unknown parameters are deterministic, the Fisher information is local, specified at a fixed parameter realization (denoted by $\mathbf{J}^{(D)}(\boldsymbol{\theta})$). When the unknown parameters are random, the Bayesian CRB is relevant; the associated Fisher information includes a parameter-averaged local FIM term and an *a priori* parameter information term [7]

$$\mathbf{J} = \mathrm{E}_{\boldsymbol{\theta}} \left[\mathbf{J}^{(D)}(\boldsymbol{\theta}) \right] + \mathbf{J}_{\boldsymbol{\theta}}^{(A)} \tag{26}$$

For example, if $\boldsymbol{\theta}$ is multivariate Gaussian with covariance matrix $\mathbf{K}_{\boldsymbol{\theta}}$, the prior information term $[\mathbf{J}_{\boldsymbol{\theta}}^{(A)}]$ equals $\mathbf{K}_{\boldsymbol{\theta}}^{-1}$.

Often, the parameter set includes both deterministic and random parameters, for which a hybrid bound has been developed [7], [11]. Writing $\boldsymbol{\theta}$ in terms of its two independent subsets, $\boldsymbol{\theta} = \{\boldsymbol{\theta}_{\mathrm{det}}, \boldsymbol{\theta}_{\mathrm{ram}}\}$, the hybrid Fisher information is given by

$$\mathbf{J} = \begin{bmatrix} \mathrm{E}_{\boldsymbol{\theta}_{\mathrm{ram}}} \left[\mathbf{J}_{\boldsymbol{\theta}_{\mathrm{det}}}^{(D)} \right] & \mathrm{E}_{\boldsymbol{\theta}_{\mathrm{ram}}} \left[\mathbf{J}_{\boldsymbol{\theta}_{\mathrm{det}} \boldsymbol{\theta}_{\mathrm{ram}}}^{(D)} \right]^T \\ \mathrm{E}_{\boldsymbol{\theta}_{\mathrm{ram}}} \left[\mathbf{J}_{\boldsymbol{\theta}_{\mathrm{det}} \boldsymbol{\theta}_{\mathrm{ram}}}^{(D)} \right] & \mathrm{E}_{\boldsymbol{\theta}_{\mathrm{ram}}} \left[\mathbf{J}_{\boldsymbol{\theta}_{\mathrm{ram}}}^{(D)} \right] \end{bmatrix} + \begin{bmatrix} \mathbf{0} & \mathbf{0}'^T \\ \mathbf{0}' & \mathbf{J}_{\boldsymbol{\theta}_{\mathrm{ram}}}^{(A)} \end{bmatrix} \tag{27}$$

where $\mathbf{J}_{\boldsymbol{\theta}_{\mathrm{det}}}^{(D)}$ and $\mathbf{J}_{\boldsymbol{\theta}_{\mathrm{ram}}}^{(D)}$ are the local Fisher information for $\boldsymbol{\theta}_{\mathrm{det}}$ and $\boldsymbol{\theta}_{\mathrm{ram}}$, respectively; $\mathbf{J}_{\boldsymbol{\theta}_{\mathrm{det}} \boldsymbol{\theta}_{\mathrm{ram}}}^{(D)}$ is their coupling term; $\mathbf{0}$ and $\mathbf{0}'$ are all-zero matrices with their sizes defined accordingly; and $\mathbf{J}_{\boldsymbol{\theta}_{\mathrm{ram}}}^{(A)}$ is the *a priori* Fisher information.

The off-diagonal term of the CRB matrix is an indication of parameter coupling, which specifies how the error in the estimation of one parameter correlates with the error in the estimation of another parameter [12], i.e., the error coupling at the system output end. A typical quantitative coupling measure is defined by

$$\rho_{ij}^2 = \frac{\left| \left[\mathbf{J}^{-1} \right]_{ij} \right|^2}{\left[\mathbf{J}^{-1} \right]_{ii} \left[\mathbf{J}^{-1} \right]_{jj}} \tag{28}$$

which obviously falls between 0 and 1. Note that when the CRB is achieved (as in the case of MLE at high SNR), the coupling specified by the CRB is truly the error coupling in the estimation; thus, diagonalizing the CRB matrix indeed decouples the errors in the estimation of chosen parameters, which is exploited in the development in Section IV.

B. Fisher Information in the Matched-Field Problem

The discussions in the sequel are constrained to the single-frequency case. For the usual matched-field source localization or tomography problem, the source is assumed to be a stationary random process. The complex envelope of the received signal can be expressed as [13]

$$\mathbf{r}(f_0, \boldsymbol{\theta}) = \tilde{b}(f_0) \mathbf{g}(f_0, \boldsymbol{\theta}) + \mathbf{n}(f_0) \tag{29}$$

where $\mathbf{r}(f_0, \boldsymbol{\theta})$ is an $M \times 1$ vector (recall that M is the number of receiving sensors); f_0 is the signal frequency of interest; θ

$$\mathbf{g}(r_s, z_s, \bar{\mathbf{w}}) = [g(z_1; r_s, z_s, \bar{\mathbf{w}}) \quad \dots \quad g(z_m; r_s, z_s, \bar{\mathbf{w}}) \quad \dots \quad g(z_M; r_s, z_s, \bar{\mathbf{w}})]^T \tag{18}$$

$$\mathbf{U}_0 = \begin{bmatrix} \varphi_1^{(0)}(z_1) & \cdots & \varphi_n^{(0)}(z_1) & \cdots & \varphi_N^{(0)}(z_1) \\ \vdots & \ddots & \vdots & \ddots & \vdots \\ \varphi_1^{(0)}(z_m) & \cdots & \varphi_n^{(0)}(z_m) & \cdots & \varphi_N^{(0)}(z_m) \\ \vdots & \ddots & \vdots & \ddots & \vdots \\ \varphi_1^{(0)}(z_M) & \cdots & \varphi_n^{(0)}(z_M) & \cdots & \varphi_N^{(0)}(z_M) \end{bmatrix} \tag{19}$$

$$\mathbf{S}_0(r_s, z_s) = \begin{bmatrix} \sqrt{2\pi} \frac{\varphi_1^{(0)}(z_s)}{\sqrt{k_1^{(0)} r_s}} e^{j k_1^{(0)} r_s - \delta_1^{(0)} r_s} & 0 & \cdots \\ \vdots & \ddots & \vdots \\ \cdots & 0 & \sqrt{2\pi} \frac{\varphi_N^{(0)}(z_s)}{\sqrt{k_N^{(0)} r_s}} e^{j k_N^{(0)} r_s - \delta_N^{(0)} r_s} \end{bmatrix} \tag{20}$$

includes the unknown source/environmental parameters (e.g., $\boldsymbol{\theta} = \{r_s, z_s, \bar{\mathbf{w}}\}$); $\tilde{b}(f_0)$ is a random process incorporating amplitude and phase variability of the source; $\mathbf{g}(f_0, \boldsymbol{\theta})$ is a vector of Green's function for the propagation from the source to the receiving sensors; and $\mathbf{n}(f_0)$ is the stationary noise vector.

Both the signal and noise terms are assumed to follow a zero-mean complex Gaussian distribution and the noise is independent of the signal process as well as the parameter set. In the absence of strong interferences, this assumption is reasonable when the total field environmental-dependence is dominated by that of the source signal propagation. Accordingly, the noise is spatially white, uncorrelated across sensors.

Given the matched-field data model in (29), an expression of the local Fisher information is available based on the results in [13]

$$\left[\mathbf{J}^{(D)}(\boldsymbol{\theta})\right]_{ij} = \sigma_b^4 \gamma(\boldsymbol{\theta}) \left(\mathrm{Re}\left[d^2(\boldsymbol{\theta}) v_{ij}(\boldsymbol{\theta}) - v_i(\boldsymbol{\theta}) v_j^H(\boldsymbol{\theta})\right] + \gamma(\boldsymbol{\theta}) \mathrm{Re}\left[v_i(\boldsymbol{\theta})\right] \mathrm{Re}\left[v_j(\boldsymbol{\theta})\right]\right) \quad (30)$$

where $d^2(\boldsymbol{\theta}) = (1/\sigma_n^2)\mathbf{g}^H(\boldsymbol{\theta})\mathbf{g}(\boldsymbol{\theta})$ is the SNR for the Green's function referenced in the space of the additive noise; $v_i(\boldsymbol{\theta}) = (1/\sigma_n^2)\mathbf{g}^H(\boldsymbol{\theta})((\partial/\partial\theta_i)\mathbf{g}(\boldsymbol{\theta}))$ is a measure of the mean of the parameter sensitivity in the same space; $v_{ij}(\boldsymbol{\theta}) = (1/\sigma_n^2)((\partial/\partial\theta_i)\mathbf{g}^H(\boldsymbol{\theta}))((\partial/\partial\theta_j)\mathbf{g}(\boldsymbol{\theta}))$ is a measure of the convexity of the parameter sensitivity; $\gamma(\boldsymbol{\theta}) = 2/(1+\sigma_b^2 d^2(\boldsymbol{\theta}))$; σ_b^2 is the variance of the signal process; σ_n^2 is the variance of the noise process; and $()^H$ denotes the complex conjugate transpose operation. Clearly the local information matrix is determined from the shape of the ambiguity mainlobe, i.e., the slope and curvature of the signal correlation at the true parameter point.

One should be aware that the local performance often depends on specific environments as well as specific parameter values, and the ocean environment often shows strong error inhomogeneity and coupling variability over a wide range of parameter values. In such scenarios, a Bayesian bound bounds the mean-square error and the error coupling averaged over the prior parameter space.

IV. Basis Functions in Sound Speed Profile Estimation

In this section, the problem of SSP estimation is considered and the Bayesian CRB is applied. The derivations are based on the matched-field data model in (29) with the Green's function given by (17). Specifically, the CRB is derived for an arbitrary basis set in (8) and then a special transform matrix $\mathbf{E}$ is chosen so that the CRB matrix is diagonal. For simultaneous source location and SSP estimation a hybrid CRB is often assumed, which is addressed in Section VI.

As discussed in Section II-B, a multivariate Gaussian distribution is assumed for the SSP coefficients, $\bar{\mathbf{w}}$. Equation (9) specifies that

$$\Delta\bar{\mathbf{c}} = \boldsymbol{\Psi}_{\mathrm{EOF}} \mathbf{E} \bar{\mathbf{w}}. \quad (31)$$

Hence, the covariance matrix of $\bar{\mathbf{w}}$ can be derived from $\mathbf{K}_{\Delta\bar{\mathbf{c}}}$

$$\mathbf{K}_{\bar{\mathbf{w}}} = \mathbf{E}^T \boldsymbol{\Psi}_{\mathrm{EOF}}^T \mathbf{K}_{\Delta\bar{\mathbf{c}}} \boldsymbol{\Psi}_{\mathrm{EOF}} \mathbf{E}. \quad (32)$$

When the EOF set is used ($\mathbf{E} = \mathbf{I}$), $\mathbf{K}_{\bar{\mathbf{w}}}$ is the diagonal eigenvalue matrix $\boldsymbol{\Lambda}_{\mathrm{EOF}}$ in (7), which says $\bar{w}_l, l = 1, \ldots, L$, are mutually independent. For an arbitrary $\mathbf{E} \neq \mathbf{I}$, however, $\mathbf{K}_{\bar{\mathbf{w}}}$ is no longer diagonal, yielding correlated $\bar{w}_l$'s.

A. Range-Dependent Case

Under the assumption that the receiving array fully spans the water column, an analytical closed-form expression for the Fisher Information is derived in Appendix A, and the result is stated by

$$\mathbf{J} = \mathbf{E}^T \boldsymbol{\Psi}_{\mathrm{EOF}}^T \mathbf{F} \mathbf{B} \mathbf{F}^T \boldsymbol{\Psi}_{\mathrm{EOF}} \mathbf{E} + \mathbf{E}^T \left(\boldsymbol{\Psi}_{\mathrm{EOF}}^T \mathbf{K}_{\Delta\bar{\mathbf{c}}} \boldsymbol{\Psi}_{\mathrm{EOF}}\right)^{-1} \mathbf{E} \quad (33)$$

where

$$\mathbf{B} = \frac{\frac{2\sigma_b^4}{\sigma_n^4}}{1 + \frac{\sigma_b^2}{\sigma_n^2 \Delta d} \mathbf{1}^T \mathbf{S} \mathbf{1}} (\mathbf{S}\mathbf{1}^T \mathbf{S}\mathbf{1} - \mathbf{S}\mathbf{1}^T \mathbf{1}\mathbf{S}) \quad (34)$$

$$\mathbf{S} = \mathbf{S}_0^H \mathbf{S}_0 = \begin{bmatrix} 2\pi \frac{\left|\varphi_1^{(0)}(z_s)\right|^2}{k_1^{(0)} r_s} e^{-2\delta_1^{(0)} r_s} & 0 & \cdots \\ \vdots & \ddots & \vdots \\ \cdots & 0 & 2\pi \frac{\left|\varphi_N^{(0)}(z_s)\right|^2}{k_N^{(0)} r_s} e^{-2\delta_N^{(0)} r_s} \end{bmatrix} \quad (35)$$

and $\mathbf{1}$ is an $N \times 1$ all-one vector.

Inverse of (33) generates the CRB matrix. To make the CRB matrix diagonal, we only need to make the FIM diagonal. Notice that (33) can be rewritten in a more compact form

$$\mathbf{J} = \mathbf{E}^T \left(\boldsymbol{\Psi}_{\mathrm{EOF}}^T \mathbf{F} \mathbf{B} \mathbf{F}^T \boldsymbol{\Psi}_{\mathrm{EOF}} + (\boldsymbol{\Psi}_{\mathrm{EOF}}^T \mathbf{K}_{\Delta\bar{\mathbf{c}}} \boldsymbol{\Psi}_{\mathrm{EOF}})^{-1}\right) \mathbf{E}. \quad (36)$$

The desired transform matrix, denoted by $\mathbf{E}_{\mathrm{SOF}}$, is readily solved from an eigendecomposition problem, i.e., the eigenvectors of the matrix

$$\boldsymbol{\Psi}_{\mathrm{EOF}}^T \mathbf{F} \mathbf{B} \mathbf{F}^T \boldsymbol{\Psi}_{\mathrm{EOF}} + \left(\boldsymbol{\Psi}_{\mathrm{EOF}}^T \mathbf{K}_{\Delta\bar{\mathbf{c}}} \boldsymbol{\Psi}_{\mathrm{EOF}}\right)^{-1}. \quad (37)$$

The new set of SSP basis functions is then obtained by $\boldsymbol{\Psi}_{\mathrm{SOF}} = \boldsymbol{\Psi}_{\mathrm{EOF}} \mathbf{E}_{\mathrm{SOF}}$.

Clearly, the new basis functions depend on not only the statistics of the SSP uncertainty, $\mathbf{K}_{\Delta\bar{\mathbf{c}}}$, but also the propagation of the environmental property through the waveguide system including the signal receiving system as embedded in $\mathbf{F}$ and $\mathbf{B}$. They also include the SNR in measurements through the term of $\mathbf{B}$. Even though the detailed behavior of (37) in terms of SNR can be quite complicated, at high SNR the first term is expected to dominate; as the SNR decreases, the prior statistical information becomes important. In the same sense, when the prior information is quite accurate (small variance), the second term in (37) is expected to make more contributions.

It is interesting to note that we are actually trying to orthogonalize the retained EOFs from the system view. When a com-

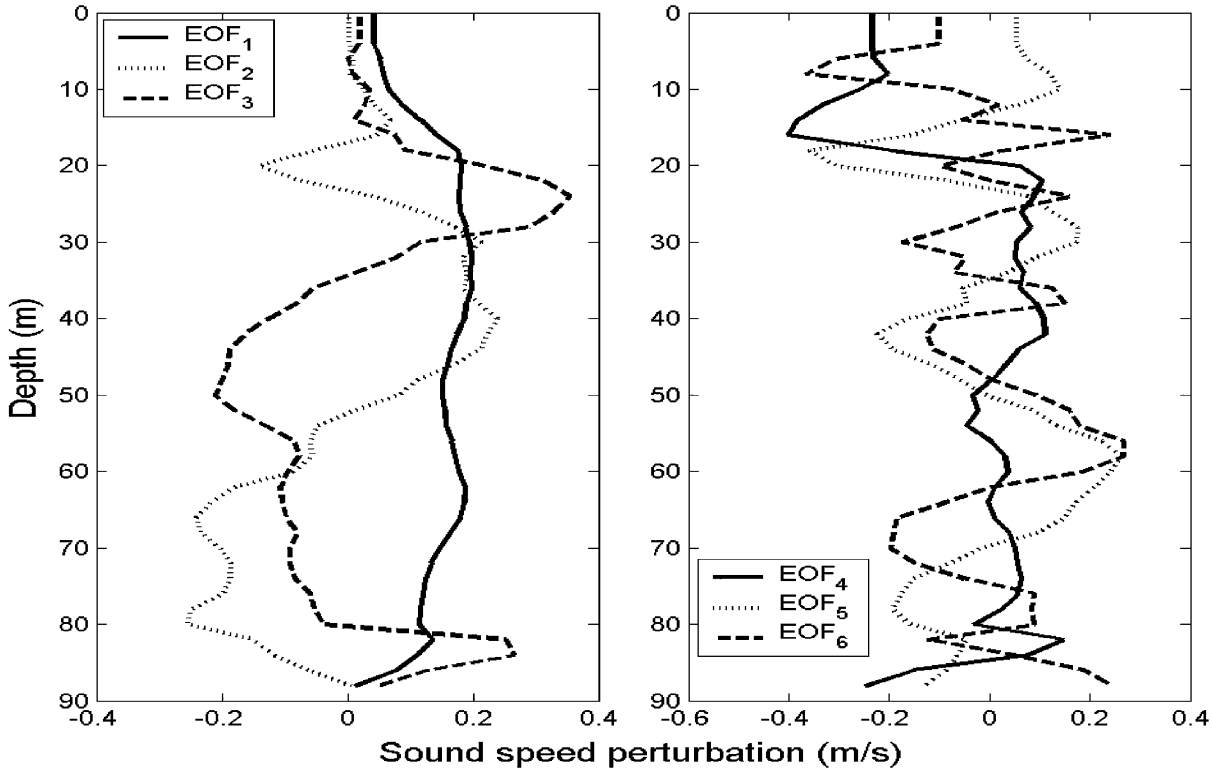

Fig. 2. Empirical orthogonal functions computed from the PRIMER onsite measurements [17].

plete EOF set is used (i.e., all the SSP statistical information is retained), (36) can be rewritten as

$$\mathbf{J} = \mathbf{E}^T \boldsymbol{\Psi}_{\mathrm{EOF}}^T \left(\mathbf{F}\mathbf{B}\mathbf{F}^T + \mathbf{K}_{\Delta \tilde{\mathbf{c}}}^{-1} \right) \boldsymbol{\Psi}_{\mathrm{EOF}} \mathbf{E} \tag{38}$$

since $\boldsymbol{\Psi}_{\mathrm{EOF}} \boldsymbol{\Psi}_{\mathrm{EOF}}^T = \boldsymbol{\Psi}_{\mathrm{EOF}}^T \boldsymbol{\Psi}_{\mathrm{EOF}} = \mathbf{I}$. Hence, $\boldsymbol{\Psi}_{\mathrm{SOF}}$ is simply the eigenvector set of the matrix (cf. (8))

$$\mathbf{F}\mathbf{B}\mathbf{F}^T + \mathbf{K}_{\Delta \tilde{\mathbf{c}}}^{-1}. \tag{39}$$

B. Range-Independent Case

For the range-independent case, the Fisher Information is derived as (cf. Appendix A)

$$\mathbf{J} = \mathbf{E}^T \left(r_s^2 \boldsymbol{\Psi}_{\mathrm{EOF}}^T \mathbf{F}\mathbf{B}\mathbf{F}^T \boldsymbol{\Psi}_{\mathrm{EOF}} + \left(\boldsymbol{\Psi}_{\mathrm{EOF}}^T \mathbf{K}_{\Delta \mathbf{c}} \boldsymbol{\Psi}_{\mathrm{EOF}} \right)^{-1} \right) \mathbf{E}. \tag{40}$$

To make this FIM associated with $\mathbf{w}$ diagonal, the transform matrix, $\mathbf{E}_{\mathrm{SOF}}$, is the eigenvector set of the matrix

$$r_s^2 \boldsymbol{\Psi}_{\mathrm{EOF}}^T \mathbf{F}\mathbf{B}\mathbf{F}^T \boldsymbol{\Psi}_{\mathrm{EOF}} + \left(\boldsymbol{\Psi}_{\mathrm{EOF}}^T \mathbf{K}_{\Delta \mathbf{c}} \boldsymbol{\Psi}_{\mathrm{EOF}} \right)^{-1}. \tag{41}$$

Note that r_s^2 can be cancelled out by some related quantities in $\mathbf{B}$. This can be understood under the range-independence assumption. The only source range-dependent term is the attenuation [cf. (35)], which can be combined into the SNR term in $\mathbf{B}(\sigma_b^2/\sigma_n^2)$.

It is worth noting that the array full-spanning assumption is not indispensable for an analytical solution in the problem. For a short array, even though (50) is no longer met, one can still derive the Fisher Information using the first lines of (51), (52), and (53). The result is similar to (36), (38), or (40), but the term between $\mathbf{E}^T$ and $\mathbf{E}$ is quite lengthy, which is omitted here.

V. Examples

To demonstrate the developed concept, we present a few shallow water examples of SSP representation. The SSP statistics comes from the shelf break PRIMER experiment, which was conducted south of New England in the Middle Atlantic Bight during summer 1996 [14]. The PRIMER site is typical of shallow water propagation, characterized by a wide range of highly variable oceanographic processes including the shelf break front, the external forcing by the nearby Gulf stream, and the nonlinear internal waves [15]. An isovelocity channel [Fig. 1(a)] is first considered, for which an exact analytical expression for sound propagation is available [9]; then, an example track from the PRIMER site [Fig. 1(b)] is studied; both environments are range-independent.

In both cases, the SSP is sampled by $N_Z = 47$ discrete depth points from the surface (0 m) to the bottom (92 m), equally spaced by 2 m. This spacing is chosen from the available SSP data measurements, and can certainly be larger for the purpose of representing either the SSP variations or the modal shape functions. For the convenience of computation, the sensors in the vertical receiving array are chosen at the same depth points as for the SSP (thus, $M = 47$). A point source at a single frequency of 100 Hz is considered, located at 18 m depth and 50 km range. For the real PRIMER track, the Kraken normal modes model [16] is used to compute the Green's function for the given mean environment and source-receiver configuration.

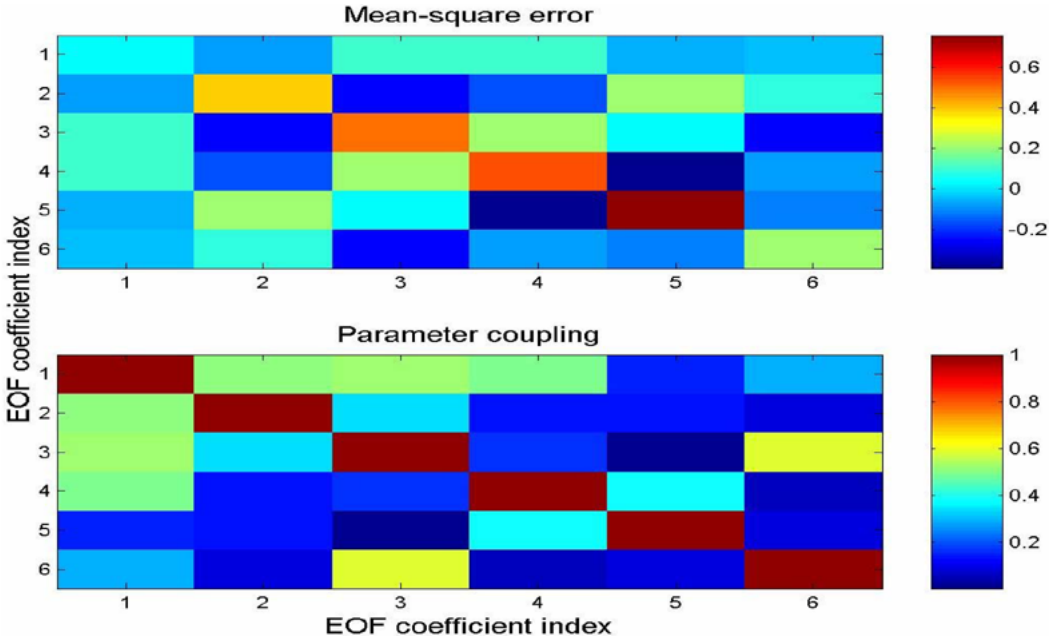

Fig. 3. Cramer–Rao bound matrix for EOF coefficient estimation under the environment of Fig. 1(a). The bottom panel is the normalized parameter coupling in (28). $\mathrm{SNR} = 0$ dB.

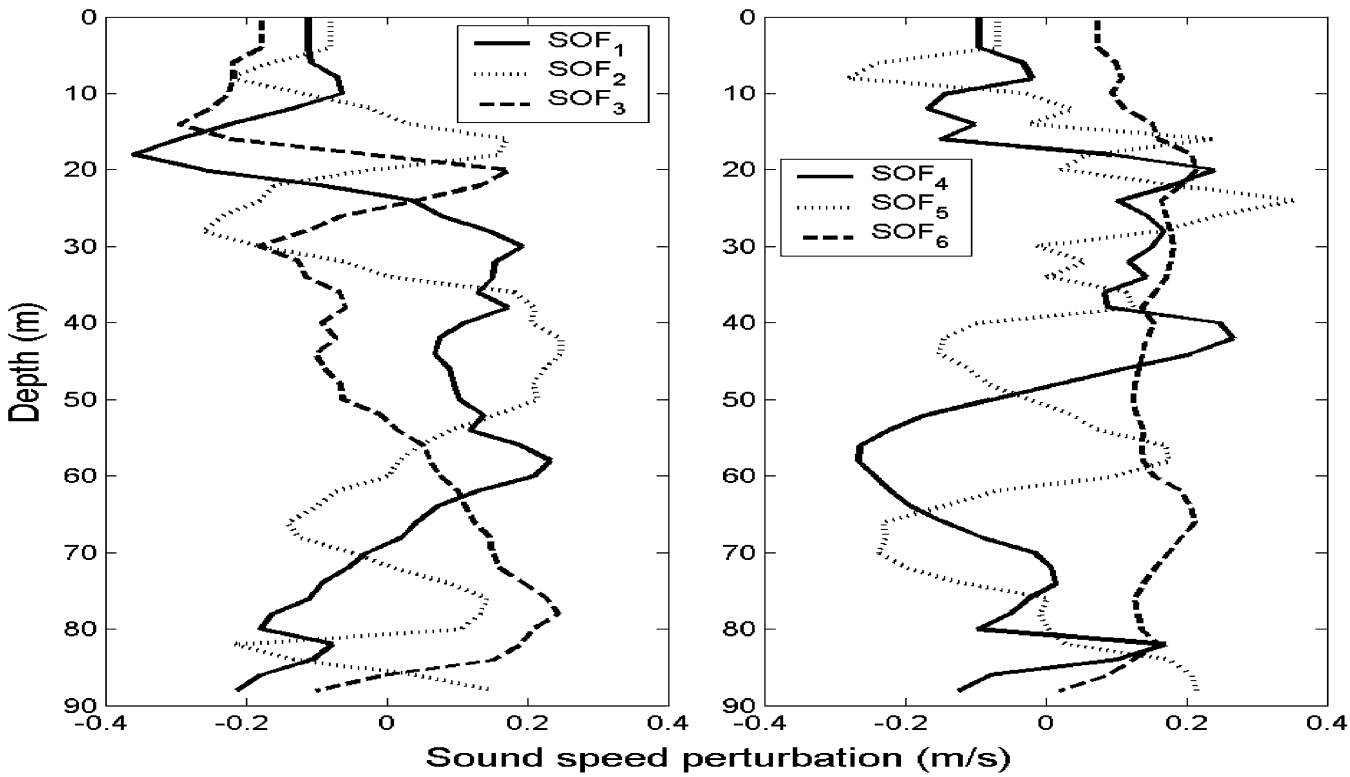

Fig. 4. System orthogonal functions under the environment of Fig. 1(a). $\mathrm{SNR} = 0$ dB.

The EOFs are computed based on the onsite sound speed measurements along the range-independent track from core 1 to 3 (cf. [14], Fig. 4). The first six EOFs are shown in Fig. 2, which, in terms of energy, describe 99.96% of the sound speed variation. The available data include 22 SSPs at 47 depth points; a diagonal loading is thus used to avoid the singularity of the covariance matrix. The sound speed variation presents highly oscillatory behavior with mid-depth peaks, which can be attributed to some complicated oceanographic processes in the studied region, for example, the internal wave. In the very top some measurement data are missing; a constant speed is used instead.

Fig. 3 displays the CRB matrix for EOF coefficients estimation under the ideal isovelocity channel [Fig. 1(a)]. The small value of individual mean-square errors is reasonable given the complete duct propagation without any bottom reflection/absorption energy loss. To better look at the parameter coupling,

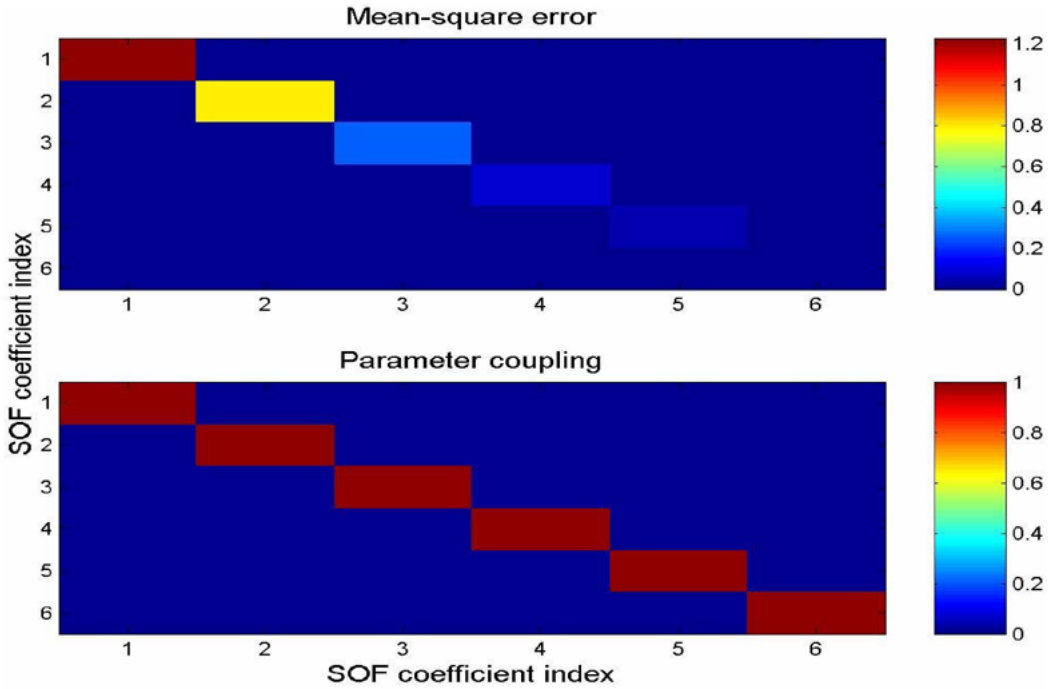

Fig. 5. Cramer–Rao bound matrix for SOF coefficient estimation under the environment of Fig. 1(a). The bottom panel is the normalized parameter coupling in (28). $\mathrm{SNR} = 0$ dB.

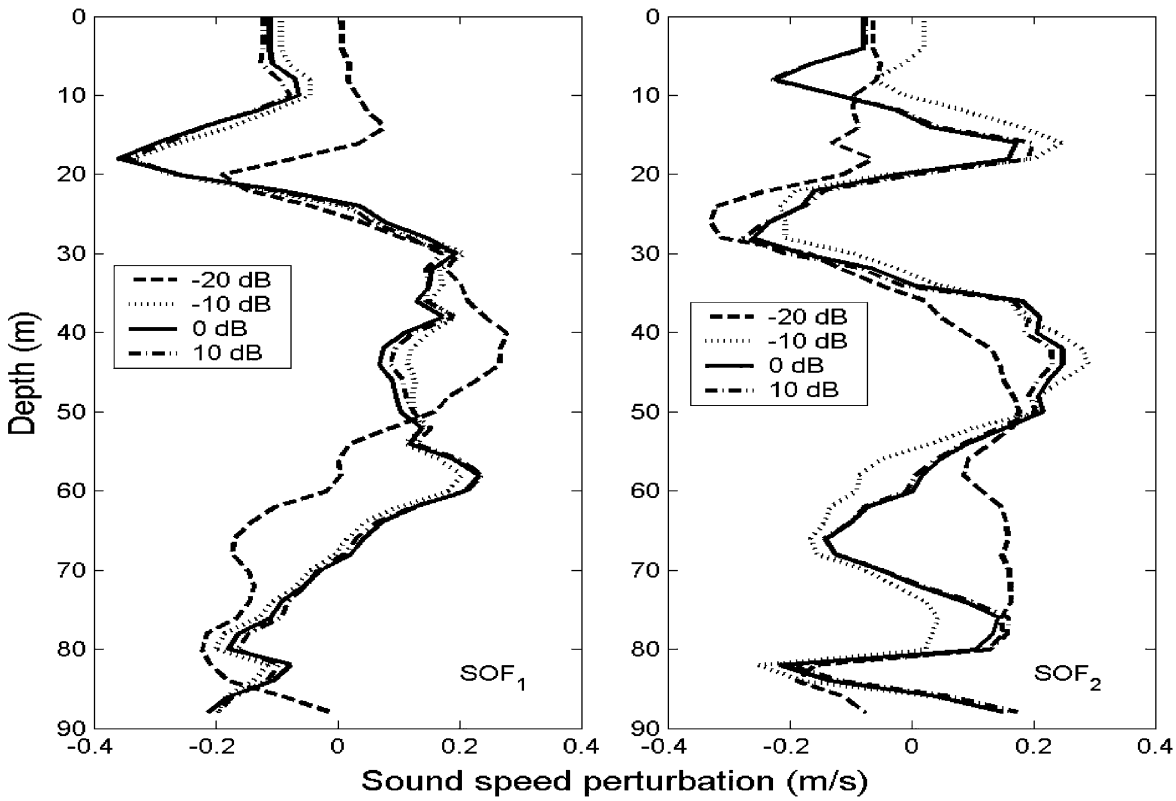

Fig. 6. System orthogonal functions at different SNRs under the environment of Fig. 1(a).

the normalized term defined in (28) is plotted in the bottom panel. Obviously, some of those errors are highly coupled, well above 0.5. As mentioned in Section I, it is thus hard to tell the relative error contributions of individual EOFs, even though the EOF_5 appears to be the most difficult one to estimate.

A new set of basis functions is obtained for the same environment using the approach developed in Section IV-B. They are shown in Fig. 4 with the corresponding CRB matrix in Fig. 5. Those functions are individually linear combinations of the EOFs, but are now mutually decoupled in terms of the estimation error. Among them, SOF_1 has the largest error, which is indeed highly correlated with EOF_5, i.e., the inner product between these two functions is high (close resemblance in depth-dependent shape). Note that SOF_6 is highly correlated

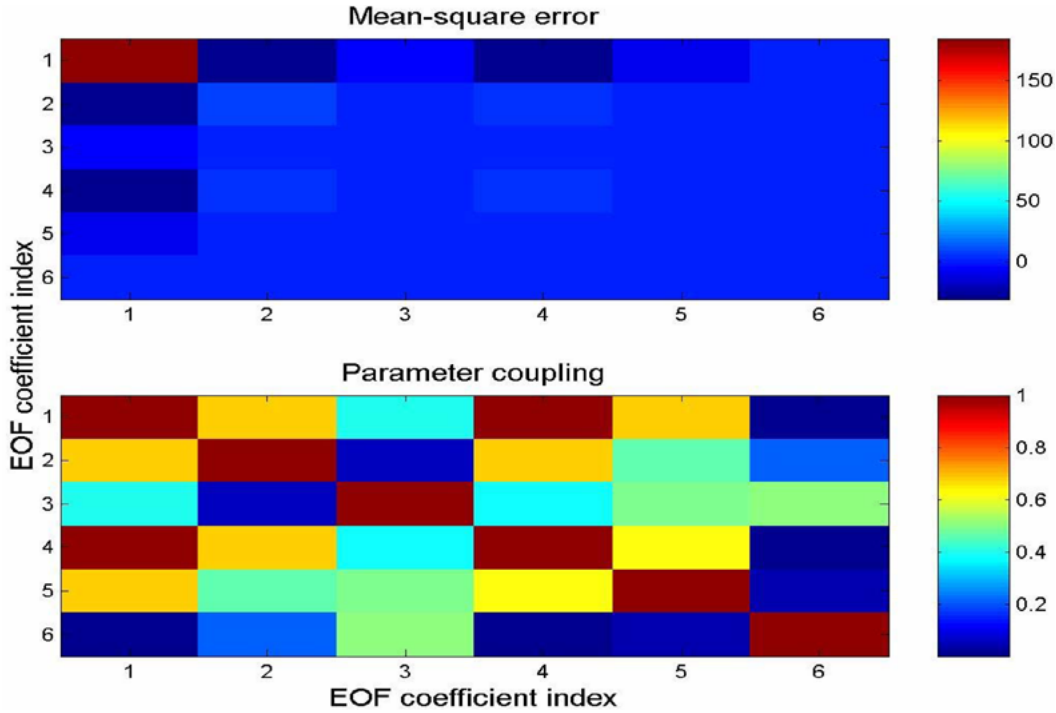

Fig. 7. Cramer–Rao bound matrix for EOF coefficient estimation under the environment of Fig. 1(b). The bottom panel is the normalized parameter coupling in (28). $\mathrm{SNR} = 0$ dB.

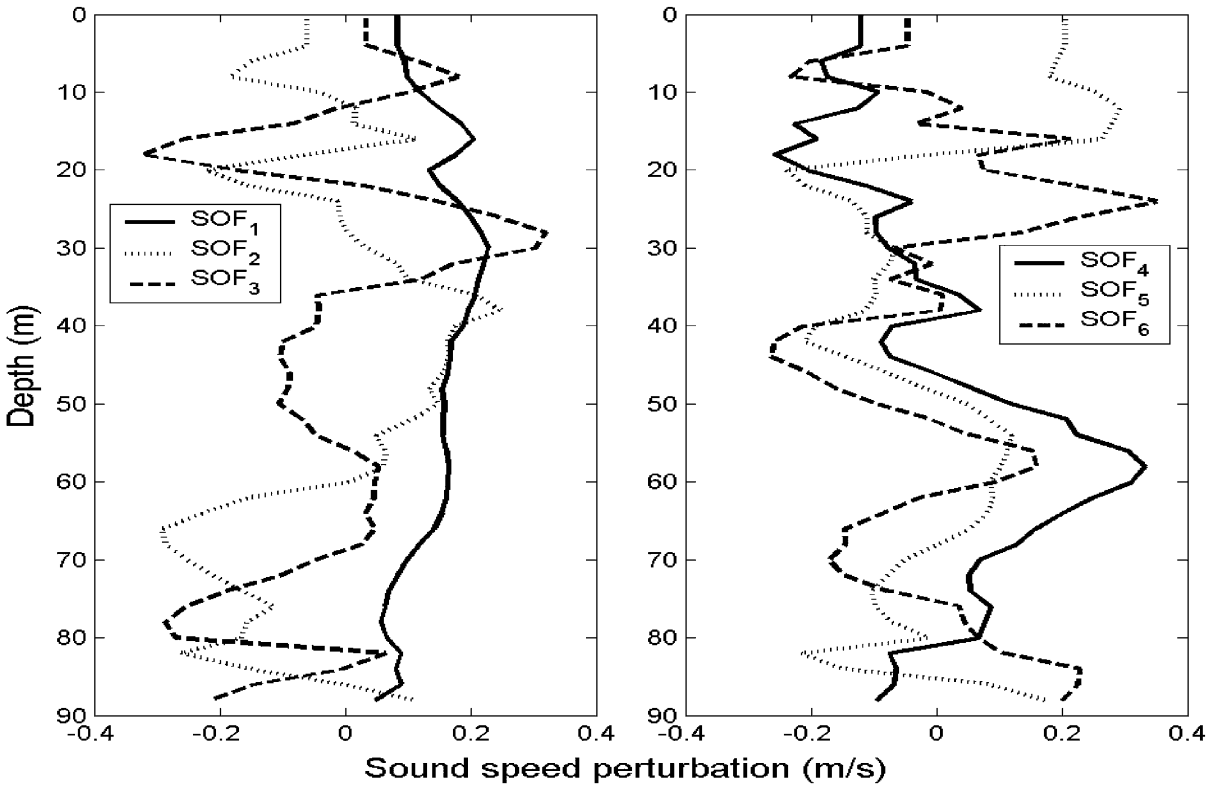

Fig. 8. System orthogonal functions under the environment of Fig. 1(b). $\mathrm{SNR} = 0$ dB.

with EOF_1; even though EOF_1 dominates the SSP variation and is thus the most uncertain one, it can actually be estimated to a high degree of accuracy. It would be very interesting to relate the derived SOFs to a specific environmental/system configuration and then explain why they are causing more or less error. This is, though, beyond the scope of the current paper.

So far the SNR is assumed to be at 0 dB defined at individual sensors averaged across the array. This is not an insignificant number considering that the array gain is about 17 dB. The SOFs include the effect of the measurement noise; in reality, however, one might want a basis set less sensitive to noise while remaining decoupled. Fortunately, as seen from Fig. 6, the SOFs differ slightly over a wide range of SNR above -10 dB. Those

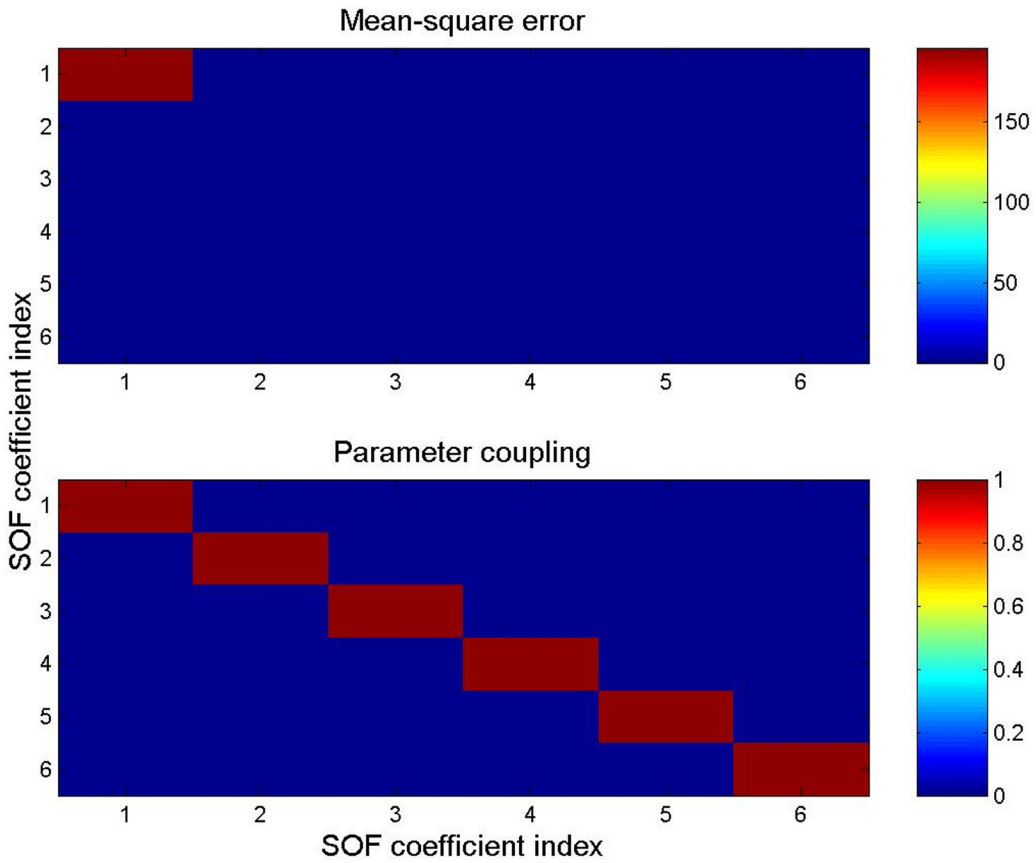

Fig. 9. Cramer–Rao bound matrix for SOF coefficient estimation under the environment of Fig. 1(b). The bottom panel is the normalized parameter coupling in (28). $\mathrm{SNR} = 0$ dB. (Color version available online at http://ieeexplore.ieee.org.)

correspond to the CRB-operation region where the asymptotic performance can be achieved by the MLE. At $\mathrm{SNR} = -20$ dB, some significant difference is observed, showing that the *a priori* SSP information (EOFs) becomes important as the noise level increases. (Each SOF is in close resemblance with one of the EOFs).

The environmental model in Fig. 1(b) is based on tomographic inversion of sediment properties along the same track [14] measuring the SSP. At source depth, the water column has a strongly downward refraction SSP, which is then almost isovelocity in the bottom half with a few local minor ducts. A strong bottom interaction is expected, which, together with the sediment attenuation, makes the signal field smeared out in terms of the resolvability of individual EOFs. This is seen from the CRB matrix in Fig. 7. The estimation errors are much larger compared to those in Fig. 3. Some of the EOFs are highly coupled in the estimation, for example, EOF_1 and EOF_4. On the contrary, the derived SOFs (Fig. 8) are decoupled as seen from the CRB matrix (Fig. 9). Note that the first few EOFs dominate the estimation error. The first three SOFs are highly correlated with the corresponding EOFs but with some slight modification the SOFs are able to decouple the errors in the estimation. The error is now nearly compacted to the first SOF coefficient as a result of decoupling.

VI. Further Discussions

Parameter coupling in the matched-field problem is often introduced by the waveguide sound propagation physics [12]. *A priori* analysis of a particular application scenario by the CRB discloses such properties. Even though a practical environmental inversion technique may not achieve the CRB, we expect that the error coupling, imposed by the same physical rule, can still be described by the CRB, and thus the development in this paper applies.

In the framework of acoustic data assimilation, the matched-field tomography approach to sound speed field estimation is generalized to include a variety of sources of information of interest such as an oceanographic model of sound speed field, direct local sound speed measurements, and a full filed acoustic propagation model as well as measurements [4]; the strengths of individual data types, e.g., the large coverage of integral acoustic measurements and the high resolution of local direct measurements, can then all be exploited. The system orthogonal function approach helps identify prominent sound speed perturbation features (associated with individual basis functions), thus facilitating optimum deployment of environmental assessment resources, otherwise limited, for local measurements. For examples, if a particular system determines certain SOFs are important, they are to be represented well in the environmental sampling scheme; the oceanographic model assimilates the local measurements to improve large-scale sound speed field prediction, which is then used to reduce the SSP estimation error by the same system defining the SOFs.

Environmental parameter estimation is often addressed in the context of source localization as well. For a physical model-based method such as matched-field processing, environmental uncertainty is the main limiting factor to achieve the performance such method is designed to achieve under

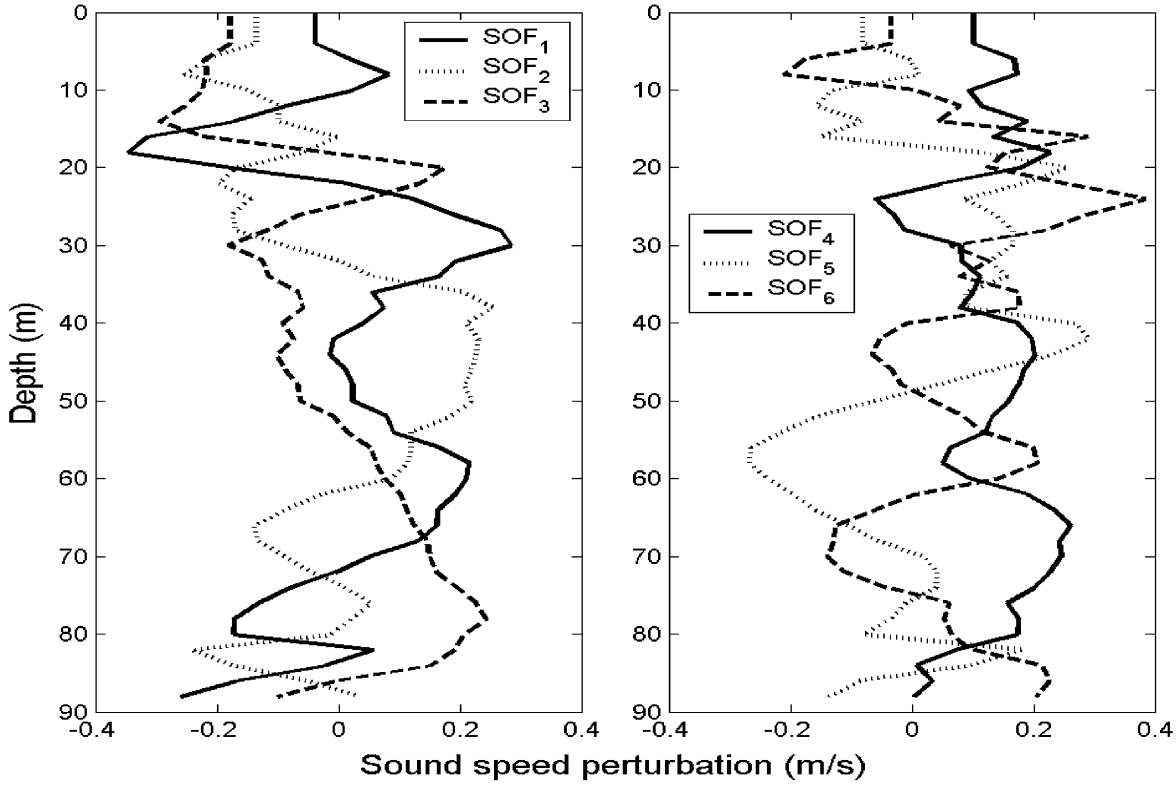

Fig. 10. System orthogonal functions under the environment of Fig. 1(a) with source range simultaneously estimated. $\mathrm{SNR} = 0$ dB.

ideal conditions. In a typical implementation, an environmental/system model is assumed and some of the parameters values are assigned per one's best knowledge on the test site. It is very common that this assumed model differs from the true one, leading to biased source location estimates even at high SNR. To deal with this mismatch problem, a common technique is to implement concurrent source localization and environmental inversion, which involves identifying environmental features critical to source localization and reducing their forecast uncertainty using, for example, the data assimilation approach. Issues on the choice of environmental parameterization can then be much different from the sole environmental parameter estimation problem.

Consider, for example, simultaneous source range and SSP coefficient estimation in a range independent channel. The source range is assumed as deterministic but unknown. The hybrid Fisher information in (27) is thus applicable and derived as (42), as shown at the bottom of the page, (cf. Appendix B), where $\mathrm{tr}()$ is the trace operation, and

$$\mathbf{k}_{\mathrm{H}} = \left[k_1^{(0)} + j\delta_1^{(0)} + j\frac{1}{2r_s}, \quad \ldots, \quad k_N^{(0)} + j\delta_N^{(0)} + j\frac{1}{2r_s}\right]^{\mathrm{T}}. \tag{43}$$

The hybrid CRB matrix can be written as

$$\mathbf{CRB} = \begin{bmatrix} \mathbf{CRB}_r & \mathbf{CRB}_{r\mathbf{w}}^T \\ \mathbf{CRB}_{r\mathbf{w}} & \mathbf{CRB}_{\mathbf{ww}} \end{bmatrix} = \mathbf{J}^{-1}. \tag{44}$$

To decouple the SSP coefficients as done in Section IV, we need to make $\mathbf{CRB}_{\mathbf{ww}}$ diagonal. Using the matrix inversion result in ([6], p. 572), we have

$$\begin{aligned}\mathbf{CRB}_{\mathbf{ww}} = \mathbf{E}^T \Big(& r_s^2 \mathbf{\Psi}_{\mathrm{EOF}}^T \mathbf{F}\mathbf{B}\mathbf{F}^T \mathbf{\Psi}_{\mathrm{EOF}} \\ & + \left(\mathbf{\Psi}_{\mathrm{EOF}}^T \mathbf{K}_{\Delta\mathbf{c}} \mathbf{\Psi}_{\mathrm{EOF}}\right)^{-1} \\ & - \frac{r_s^2}{\alpha} \mathbf{\Psi}_{\mathrm{EOF}}^T \mathbf{F}\mathbf{B}\mathbf{k}_{\mathrm{H}}\mathbf{k}_{\mathrm{H}}^T\mathbf{B}\mathbf{F}^T\mathbf{\Psi}_{\mathrm{EOF}} \Big)^{-1} \mathbf{E}. \end{aligned} \tag{45}$$

The desired transform matrix $\mathbf{E}_{\mathrm{SOF}}$ is then given by the eigenvector set of the matrix

$$\begin{aligned}\Big(& r_s^2 \mathbf{\Psi}_{\mathrm{EOF}}^T \mathbf{F}\mathbf{B}\mathbf{F}^T \mathbf{\Psi}_{\mathrm{EOF}} + (\mathbf{\Psi}_{\mathrm{EOF}}^T \mathbf{K}_{\Delta\mathbf{c}} \mathbf{\Psi}_{\mathrm{EOF}})^{-1} \\ & - \frac{r_s^2}{\alpha} \mathbf{\Psi}_{\mathrm{EOF}}^T \mathbf{F}\mathbf{B}\mathbf{k}_{\mathrm{H}}\mathbf{k}_{\mathrm{H}}^T\mathbf{B}\mathbf{F}^T\mathbf{\Psi}_{\mathrm{EOF}} \Big)^{-1}. \end{aligned} \tag{46}$$

Comparing (46) to (41), we now have the contribution from the coupling between source range and SSP coefficients. Fig. 10 displays the SOFs under the environment of Fig. 1(a). They are quite similar to the previous ones with source range exactly known (cf. Fig. 4), except a new SOF_4 replacing the previous SOF_6. Indeed, this new SOF_4 has a strong coupling with source range, as shown in Fig. 11(b).

$$\mathbf{J} = \begin{bmatrix} \mathbf{k}_{\mathrm{H}}^T\mathbf{B}\mathbf{k}_{\mathrm{H}} + \mathrm{tr}\left[\mathbf{B}\mathbf{F}^T\mathbf{\Psi}_{\mathrm{EOF}}\mathbf{\Psi}_{\mathrm{EOF}}^T\mathbf{K}_{\Delta\mathbf{c}}\mathbf{\Psi}_{\mathrm{EOF}}\mathbf{\Psi}_{\mathrm{EOF}}^T\mathbf{F}\right] & r_s\mathbf{k}_{\mathrm{H}}^T\mathbf{B}\mathbf{F}^T\mathbf{\Psi}_{\mathrm{EOF}}\mathbf{E} \\ r_s\mathbf{E}^T\mathbf{\Psi}_{\mathrm{EOF}}^T\mathbf{F}\mathbf{B}\mathbf{k}_{\mathrm{H}} & \mathbf{E}^T\left(r_s^2\mathbf{\Psi}_{\mathrm{EOF}}^T\mathbf{F}\mathbf{B}\mathbf{F}^T\mathbf{\Psi}_{\mathrm{EOF}} + (\mathbf{\Psi}_{\mathrm{EOF}}^T\mathbf{K}_{\Delta\mathbf{c}}\mathbf{\Psi}_{\mathrm{EOF}})^{-1}\right)\mathbf{E} \end{bmatrix} \tag{42}$$

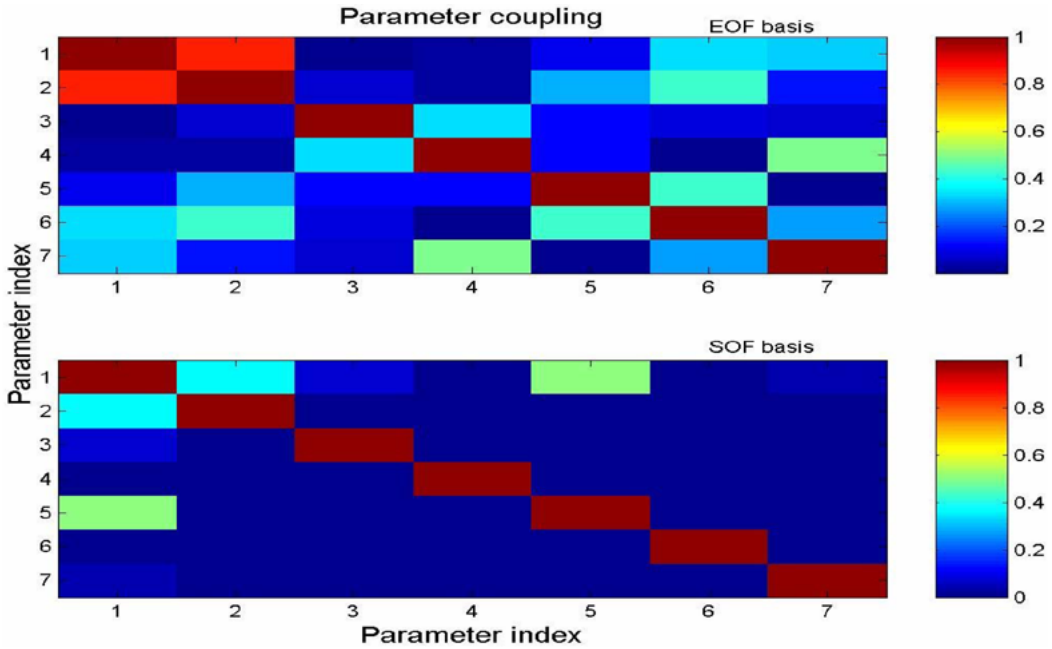

Fig. 11. Normalized parameter coupling in simultaneous source range and SSP coefficient estimation under the environment of Fig. 1(a): EOFs (top); SOFs (bottom). $\mathrm{SNR} = 0$ dB. Parameter 1 corresponds to source range; parameters 2–7 correspond to the first six SSP coefficients.

For the purpose of source localization, however, some other interesting physical interpretations are available from the CRB matrix in (44). Recall that the off-diagonal submatrix describes the error coupling between source range estimation and perturbation coefficients estimation. To obtain a robust estimation of source range, insensitive to sound speed estimation error, the orthogonal basis should be chosen so that $\mathbf{CRB}_{r\mathbf{w}}$ is close to $\mathbf{0}$. On the other side, if $\mathbf{E}$ is chosen such that $\mathbf{CRB}_{r\mathbf{w}}$ is close to $\mathbf{1}$, the source range estimation error can be reduced with reduced uncertainty in SSP. This is a desired feature in adaptive rapid environmental assessment. To limit the degree of freedom, one may want a compact size of such environmental parameter set. Thus, in reference to (42) some of columns in $\mathbf{E}$ are colinear to $\mathbf{\Psi}_{\mathrm{EOF}}^T\mathbf{F}\mathbf{B}\mathbf{k}_{\mathrm{H}}$, while the rest are orthogonal to $\mathbf{\Psi}_{\mathrm{EOF}}^T\mathbf{F}\mathbf{B}\mathbf{k}_{\mathrm{H}}$.

Due to some physical constraints, one might never find a transform matrix satisfying the exact requirements mentioned above, but some close approximations are certainly desirable, which is left for future research effort. In fact, the concept is well demonstrated even with the system-orthogonal functions developed. As seen from Fig. 11, three EOF coefficients are strongly coupled with source range (their coupling coefficients are above 0.3 while the rest below 0.1). Using the SOFs, only two are strongly coupled with source range in the same sense, and those two are mutually decoupled.

VII. Conclusion

In this paper, a new concept for system-optimal environmental parameterization is developed. Specifically, a new set of basis functions have been derived to represent the SSP in water column. Compared to the traditional EOFs, the new function set decouples the errors in the estimation of the expansion coefficients. It depends on both the statistics of the sound speed uncertainty and the sound waveguide propagation property, and includes the measurement noise as well even though simulations show those functions are quite similar at high SNRs. The analytical, closed-form solution is obtained under the adiabatically range-dependent environment; for more general cases, some numerical approach may need to be exploited.

Using such system-orthogonal basis functions reduces the degrees of freedom in environmental uncertainty modeling; it also makes possible the investigation of the relative significance of the individual basis functions in system response, thus simplifying the design of optimal adaptive sampling of environment. Fundamentally, the new development provides a framework to connect oceanographic parameterization to sonar modeling and potentially to end-user modeling.

Following the concept developed here, some other interesting results are expected, for example, basis functions coupled/uncoupled to source parameters as discussed in Section VI. In addition, a more realistic sound speed model involving 2-D (range and depth) basis functions, potentially feature related (like those characterizing the surface and internal wave effects [8]), may be applied. Furthermore, since the perturbation theory applies to many other parameters [10], a comprehensive basis set for environmental parameters including those sediment ones can be developed in a straightforward way.

Appendix
Derivation of the Fisher Information Matrix

A. SSP Coefficient Estimation Only

We first derive the derivative of the Green's function with respect to $\bar{w}_l$. Denote from (16)

$$\mathbf{Q} = \begin{bmatrix} e^{j\Delta\Theta_1} & \cdots & \cdots & \cdots \\ \vdots & e^{j\Delta\Theta_2} & \ddots & \vdots \\ \vdots & \ddots & \ddots & \vdots \\ \vdots & \cdots & \cdots & e^{j\Delta\Theta_N} \end{bmatrix} \tag{47}$$

and

$$\mathbf{E} = [\mathbf{e}_1 \quad \ldots \quad \mathbf{e}_l \quad \ldots \mathbf{e}_L]. \tag{48}$$

Then, from (17)

$$\frac{\partial}{\partial \bar{w}_l}\mathbf{g}(\bar{\mathbf{w}}) = \mathbf{U}_0\mathbf{S}_0\frac{\partial}{\partial \bar{w}_l}\mathbf{p} = j\mathbf{U}_0\mathbf{S}_0\mathbf{Q}\,\mathbf{F}^T\mathbf{\Psi}_{\mathrm{EOF}}\mathbf{e}_l. \tag{49}$$

The receiving array is assumed densely populated and spanning the entire water column; in this case, the acoustic modes sampled by the array are orthogonal with each other

$$\mathbf{U}_0^T\mathbf{U}_0 = \frac{1}{\Delta d}\mathbf{I}. \tag{50}$$

In general, given N propagation modes, the highest-order mode has N zeros, which indicates about $N/2$ oscillation cycles; thus, from the Nyquist sampling theorem, $M = N$ samples are enough to recover the modal shape function. To achieve the orthogonality of modes, however, M may have to be larger than N, e.g., $2N$.

Given the Green's function in (17) and its derivative in (49), the involved quantities in (30) are derived as follows:

$$\begin{aligned} d^2 &= \frac{1}{\sigma_n^2}\mathbf{p}^H\mathbf{S}_0^H\mathbf{U}_0^H\mathbf{U}_0\mathbf{S}_0\mathbf{p} \\ &= \frac{1}{\sigma_n^2\Delta d}\mathbf{p}^H\mathbf{S}\mathbf{p} = \frac{1}{\sigma_n^2\Delta d}\mathbf{1}^T\mathbf{S}\mathbf{1} \qquad (51) \\ v_l &= \frac{1}{\sigma_n^2}\mathbf{g}^H(\bar{\mathbf{w}})\left(\frac{\partial}{\partial \bar{w}_l}\mathbf{g}(\bar{\mathbf{w}})\right) \\ &= \frac{j}{\sigma_n^2}\mathbf{p}^H\mathbf{S}_0^H\mathbf{U}_0^H\mathbf{U}_0\mathbf{S}_0\mathbf{Q}\,\mathbf{F}^T\mathbf{\Psi}_{\mathrm{EOF}}\mathbf{e}_l \\ &= \frac{j}{\sigma_n^2\Delta d}\mathbf{1}^T\mathbf{S}\mathbf{F}^T\mathbf{\Psi}_{\mathrm{EOF}}\mathbf{e}_l \qquad (52) \\ v_{l_1,l_2} &= \frac{1}{\sigma_n^2}\left(\frac{\partial}{\partial \bar{w}_{l_1}}\mathbf{g}^H(\bar{\mathbf{w}})\right)\left(\frac{\partial}{\partial \bar{w}_{l_2}}\mathbf{g}(\bar{\mathbf{w}})\right) \\ &= \frac{1}{\sigma_n^2}\mathbf{e}_{l_1}^T\mathbf{\Psi}_{\mathrm{EOF}}^T\mathbf{F}\mathbf{Q}^H\mathbf{S}_0^H\mathbf{U}_0^T\mathbf{U}_0\mathbf{S}_0\mathbf{Q}\,\mathbf{F}^T\mathbf{\Psi}_{\mathrm{EOF}}\mathbf{e}_{l_2} \\ &= \frac{1}{\sigma_n^2\Delta d}\mathbf{e}_{l_1}^T\mathbf{\Psi}_{\mathrm{EOF}}^T\mathbf{F}\mathbf{S}\,\mathbf{F}^T\mathbf{\Psi}_{\mathrm{EOF}}\mathbf{e}_{l_2} \qquad (53) \end{aligned}$$

where $\mathbf{S}$, defined in (35), is a diagonal matrix. Note that v_l is purely imaginary.

The local Fisher information matrix is then derived by

$$\begin{aligned} \left[\mathbf{J}^{(D)}(\bar{\mathbf{w}})\right]_{l_1,l_2} &= \frac{2\sigma_b^4}{1+\sigma_b^2 d^2}\mathrm{Re}\left[d^2 v_{l_1,l_2} - v_{l_1}v_{l_2}^H\right] \\ &= \mathbf{e}_{l_1}^T\mathbf{\Psi}_{\mathrm{EOF}}^T\mathbf{F}\mathbf{B}\mathbf{F}^T\mathbf{\Psi}_{\mathrm{EOF}}\mathbf{e}_{l_2} \qquad (54) \end{aligned}$$

where $\mathbf{B}$ is defined in (34). Notice that the matrix $\mathbf{B}$ is singular since the sum of columns is a null vector. The symmetrical structure with respect to l_1 and l_2 in (54) leads to a compact form for the entire local FIM

$$\mathbf{J}^{(D)}(\bar{\mathbf{w}}) = \mathbf{E}^T\mathbf{\Psi}_{\mathrm{EOF}}^T\mathbf{F}\mathbf{B}\mathbf{F}^T\mathbf{\Psi}_{\mathrm{EOF}}\mathbf{E}. \tag{55}$$

Now we need to integrate the local Fisher information over the distribution of $\bar{\mathbf{w}}$. Fortunately, the local FIM is in fact independent of $\bar{\mathbf{w}}$, which essentially removes the integration. Thus, the total Fisher information matrix in (26) is given by

$$\mathbf{J} = \mathbf{E}^T\mathbf{\Psi}_{\mathrm{EOF}}^T\mathbf{F}\mathbf{B}\mathbf{F}^T\mathbf{\Psi}_{\mathrm{EOF}}\mathbf{E} + \mathbf{K}_{\bar{\mathbf{w}}}^{-1}. \tag{56}$$

Using the result in (32) and the orthonormality of $\mathbf{E}$, we finally reach (36).

For the range-independent case, $\Delta\mathbf{c} = \mathbf{\Psi}_{\mathrm{EOF}}\mathbf{E}\mathbf{w}$, and thus $\mathbf{K}_{\mathbf{w}} = \mathbf{E}^T\mathbf{\Psi}_{\mathrm{EOF}}^T\mathbf{K}_{\Delta\mathbf{c}}\mathbf{\Psi}_{\mathrm{EOF}}\mathbf{E}$. The derivative of the Green's function is

$$\frac{\partial}{\partial w_l}\mathbf{g}(\mathbf{w}) = jr_s\mathbf{U}_0\mathbf{S}_0\mathbf{Q}\,\mathbf{F}^T\mathbf{\Psi}_{\mathrm{EOF}}\mathbf{e}_l \tag{57}$$

where $\Delta\mathbf{\Theta}$ in $\mathbf{Q}$ is defined according to (24). Following the derivation leading to (51)–(56), the total Fisher information is obtained as shown in (40).

B. Simultaneous SSP Coefficient and Source Range Estimation

The derivative of the Green's function with respect to source range is solved from (17)

$$\begin{aligned} \frac{\partial}{\partial r_s}\mathbf{g}(r_s,\mathbf{w}) &= \mathbf{U}_0\left(\frac{\partial}{\partial r_s}\mathbf{S}_0(r_s)\right)\mathbf{p} + \mathbf{U}_0\mathbf{S}_0(r_s)\frac{\partial}{\partial r_s}\mathbf{p} \\ &= j\mathbf{U}_0\mathbf{S}_0(r_s)\mathbf{Q}\left[\mathbf{k}_{\mathrm{H}} + \mathbf{F}^T\mathbf{\Psi}_{\mathrm{EOF}}\mathbf{E}\mathbf{w}\right] \qquad (58) \end{aligned}$$

where $\mathbf{k}_{\mathrm{H}}$ is defined in (43) and the notations in Section IV are used. For long range propagation modes, the imaginary part in $\mathbf{k}_{\mathrm{H}}$ is much smaller compared to the real part and thus often ignored. Denote source range by parameter index 1 and SSP coefficients 1 to L by parameter index 2 to $L+1$. The r_s -related quantities in the FIM [cf. (30)] can be derived as

$$\begin{aligned} v_1 &= \frac{1}{\sigma_n^2}\mathbf{g}^H(r_s,\mathbf{w})\left(\frac{\partial}{\partial r_s}\mathbf{g}(r_s,\mathbf{w})\right) \\ &= \frac{j}{\sigma_n^2\Delta d}\mathbf{1}^T\mathbf{S}\left[\mathbf{k}_{\mathrm{H}} + \mathbf{F}^T\mathbf{\Psi}_{\mathrm{EOF}}\mathbf{E}\mathbf{w}\right] \qquad (59) \\ v_{1,1} &= \frac{1}{\sigma_n^2}\left(\frac{\partial}{\partial r_s}\mathbf{g}^H(r_s,\mathbf{w})\right)\left(\frac{\partial}{\partial r_s}\mathbf{g}(r_s,\mathbf{w})\right) \\ &= \frac{1}{\sigma_n^2\Delta d}\left[\mathbf{k}_{\mathrm{H}} + \mathbf{F}^T\mathbf{\Psi}_{\mathrm{EOF}}\mathbf{E}\mathbf{w}\right]^T \\ &\quad \times \mathbf{S}\left[\mathbf{k}_{\mathrm{H}} + \mathbf{F}^T\mathbf{\Psi}_{\mathrm{EOF}}\mathbf{E}\mathbf{w}\right] \qquad (60) \\ v_{1,l+1} &= \frac{1}{\sigma_n^2}\left(\frac{\partial}{\partial r_s}\mathbf{g}^H(r_s,\mathbf{w})\right)\left(\frac{\partial}{\partial w_l}\mathbf{g}(r_s,\mathbf{w})\right) \\ &= \frac{r_s}{\sigma_n^2\Delta d}\left[\mathbf{k}_{\mathrm{H}} + \mathbf{F}^T\mathbf{\Psi}_{\mathrm{EOF}}\mathbf{E}\mathbf{w}\right]^T\mathbf{S}\mathbf{F}^T\mathbf{\Psi}_{\mathrm{EOF}}\mathbf{e}_l. \qquad (61) \end{aligned}$$

The r_s -related Fisher information is then given by

$$\begin{aligned} \left[\mathbf{J}^{(D)}(r_s,\mathbf{w})\right]_{1,1} &= \left[\mathbf{k}_{\mathrm{H}} + \mathbf{F}^T\mathbf{\Psi}_{\mathrm{EOF}}\mathbf{E}\mathbf{w}\right]^T \\ &\quad \times \mathbf{B}\left[\mathbf{k}_{\mathrm{H}} + \mathbf{F}^T\mathbf{\Psi}_{\mathrm{EOF}}\mathbf{E}\mathbf{w}\right] \qquad (62) \\ \left[\mathbf{J}^{(D)}(r_s,\mathbf{w})\right]_{1,l+1} &= r_s\left[\mathbf{k}_{\mathrm{H}} + \mathbf{F}^T\mathbf{\Psi}_{\mathrm{EOF}}\mathbf{E}\mathbf{w}\right]^T \\ &\quad \times \mathbf{B}\mathbf{F}^T\mathbf{\Psi}_{\mathrm{EOF}}\mathbf{e}_l. \qquad (63) \end{aligned}$$

Recall that $\mathbf{w}$ is zero-mean Gaussian and for two arbitrary column vectors of the same length, $\mathbf{a}$ and $\mathbf{b}$,

$\mathbf{a}^T\mathbf{b} = \mathrm{tr}(\mathbf{a}^T\mathbf{b}) = \mathrm{tr}(\mathbf{b}\mathbf{a}^T)$. We can thus easily verify

$$\mathrm{E}_{\mathbf{w}}\left[\left[\mathbf{J}^{(D)}(r_s,\mathbf{w})\right]_{1,1}\right] = \mathbf{k}_{\mathrm{H}}^T\mathbf{B}\mathbf{k}_{\mathrm{H}} + \mathrm{tr}\left[\mathbf{B}\mathbf{F}^T\mathbf{\Psi}_{\mathrm{EOF}}\mathbf{\Psi}_{\mathrm{EOF}}^T\mathbf{K}_{\Delta\mathbf{c}}\mathbf{\Psi}_{\mathrm{EOF}}\mathbf{\Psi}_{\mathrm{EOF}}^T\mathbf{F}\right] \tag{64}$$

$$\mathrm{E}_{\mathbf{w}}\left[\left[\mathbf{J}^{(D)}(r_s,\mathbf{w})\right]_{1,l+1}\right] = r_s\mathbf{k}_{\mathrm{H}}^T\mathbf{B}\mathbf{F}^T\mathbf{\Psi}_{\mathrm{EOF}}\mathbf{e}_l. \tag{65}$$

The Fisher information is now solved in (42) by combining (40), (64), and (65).

ACKNOWLEDGMENT

The authors would thank Dr. G. Potty, Dr. A. Fredricks, and Dr. J. Lynch for helping the shelf break PRIMER simulation. They would also like to thank the anonymous reviewers for valuable comments.

REFERENCES

[1] A. B. Baggeroer, W. A. Kuperman, and P. N. Mikhalevsky, "An overview of matched field methods in ocean acoustics," *IEEE J. Ocean. Eng.*, vol. 18, no. 4, pp. 401–424, Oct. 1993.

[2] H. Schmidt, A. B. Baggeroer, W. A. Kuperman, and E. K. Scheer, "Environmentally tolerant beamforming for high resolution matched field processing: Deterministic mismatch," *J. Acoust. Soc. Am.*, vol. 88, no. 4, pp. 1851–1862, Oct. 1990.

[3] J. L. Krolik, "Matched-field minimum variance beamforming in a random ocean channel," *J. Acoust. Soc. Am.*, vol. 92, no. 3, pp. 1408–1419, Sep. 1992.

[4] P. Elisseeff, H. Schmidt, and W. Xu, "Ocean acoustic tomography as a data assimilation problem," *IEEE J. Ocean. Eng.*, vol. 27, no. 2, pp. 275–282, Apr. 2002.

[5] L. R. LeBlanc and F. H. Middleton, "An underwater acoustic sound velocity data model," *J. Acoust. Soc. Am.*, vol. 67, no. 6, pp. 2055–2062, Jun. 1980.

[6] S. M. Kay, *Fundamentals of Statistical Signal Processing: Estimation Theory*. Englewood Cliffs, NJ: Prentice Hall, 1993.

[7] Y. Rockah and P. M. Schultheiss, "Array shape calibration using sources in unknown locations—Part I: Far-field sources," *IEEE Trans. Acoustics, Speech, and Signal Processing*, vol. 35, no. 3, pp. 286–299, Mar. 1987.

[8] M. Deffenbaugh, "Optimal Ocean Acoustic Tomography with Moving Sources," Ph.D. dissertation, Massachusetts Inst. of Tech., Cambridge, MA, 1997.

[9] F. B. Jensen, W. A. Kuperman, M. B. Porter, and H. Schmidt, *Computational Ocean Acoustics*. New York: American Institute of Physics Press, 1994.

[10] S. D. Rajan, J. F. Lynch, and G. V. Frisk, "Perturbative inversion methods for obtaining bottom geoacoustic parameters in shallow water," *J. Acoust. Soc. Am.*, vol. 82, no. 3, pp. 998–1017, Sep. 1987.

[11] S. Narasimhan and J. L. Krolik, "Fundamental limits on acoustic source range estimation performance in uncertain ocean channel," *J. Acoust. Soc. Am.*, vol. 97, no. 1, pp. 215–226, Jan. 1995.

[12] H. Schmidt and A. B. Baggeroer, "Physics-imposed resolution and robustness issues in seismo-acoustic parameter inversion," *Full Field Inversion Methods in Ocean and Seismo-Acoustics*, pp. 85–90, 1995.

[13] A. B. Baggeroer and H. Schmidt, "Cramer-Rao bounds for matched field tomography and ocean acoustic tomography," in *Proc. Int. Conf. Acoustics, Speech, and Signal Processing (ICASSP)*, 1995, pp. 2763–2766.

[14] G. Potty, J. Miller, J. Lynch, and K. Smith, "Tomographic inversion for sediment parameters in shallow water," *J. Acoust. Soc. Amer.*, vol. 108, no. 3, pp. 973–986, Sep. 2000.

[15] J. Lynch, A. Fredricks, J. Colosi, G. Gawarkiewicz, B. Sperry, A. Newhall, and C. S. Chiu, "An overview of acoustic fluctuation results from the summer 1996 New England Shelfbreak PRIMER experiment," in *Proc. Conf. Undersea Technology*, Taipei, Taiwan, 2002.

[16] M. B. Porter, *The KRAKEN Normal Mode Program*. Washington, DC: Naval Research Laboratory, 1992.

[17] G. Potty, "Shelf Break PRIMER Experimental Data," unpublished personnal communication.

Wen Xu (SM'04) received the B.E. degree in electrical engineering from the University of Science and Technology of China, Hefei, China, in 1990, the M.S. degree in acoustics from the Institute of Acoustics, Chinese Academy of Sciences, Beijing, China, in 1993, and the Ph.D. degree in oceanographic engineering from the Massachusetts Institute of Technology (MIT), Cambridge, in 2001.

From 1993 to 1996, he was a Research Engineer at the Institute of Acoustics, Chinese Academy of Sciences. He was with the Ocean Acoustics Group, MIT, as a Research Scientist, from 2001 to 2002. He joined the RD Instruments (now Teledyne RD Instruments), San Diego, CA, as a Research Scientist, in 2003. Since then he has been Principal Investigator/Program Manager for various advanced imaging sonar projects sponsored by the Office of Naval Research (ONR), Naval Sea Systems Command (NAVSEA), and National Oceanic and Atmospheric Administration (NOAA). His research interests include statistical and array signal processing in general and in applications to sonar, radar, and communication systems.

Dr. Xu is a member of the Acoustical Society of America. He has been the Elected Chair of the IEEE Ocean Engineering Chapter at San Diego, CA, since 2004.

Henrik Schmidt received the M.S. and Ph.D. degrees in civil engineering from The Technical University of Denmark, Lyngby, Denmark, in 1974 and 1978, respectively.

From 1978 to 1982, he worked as a Research Fellow at Risoe National Laboratory in Denmark. From 1982 to 1987, he worked as Scientist and Senior Scientist at the NATO SACLANT ASW Research Centre, Italy. He has been on faculty of the Massachusetts Institute of Technology (MIT), Cambridge, since 1987. He has served as Associate Director of Research at the MIT Sea Grant College Program, from 1989 to 2002, and as the Associate Department Head, in 1994–2002. He served as the Acting Department Head of Ocean Engineering, from 2002 to 2004. Currently, he is Professor of Mechanical and Ocean Engineering at MIT. He has been Principal Investigator in two Arctic ice station experiments, and Chief Scientist for several recent, major experiments in coastal environments. He has developed numerically efficient numerical algorithms for propagation of acoustic and seismic waves in the ocean and solid earth environment, including the SAFARI code and its successor OASES which is used as a reference propagation model in more than 100 institutions around the world, including all US Navy laboratories and most major universities involved in underwater acoustics and seismic research. The OASES code is also used extensively by several private DoD contractors as part of their sonar processing, and by the oil exploration community. In recent years, he has been pioneering the development of new underwater acoustic sensing concepts for networks of small autonomous underwater vehicles (AUV). Thus, in collaboration with SACLANT Undersea Research Centre he is exploring the possibility of using AUVs for measuring the three-dimensional acoustic scattering from the seabed to detect and identify buried objects, with application to mine countermeasures and environmental management in the littoral ocean. In addition, he has been leading the development of a synergy of ocean acoustic tomography and direct sampling by autonomous underwater vehicles for observation and forecasting of ocean processes on multiple scales. He has authored many articles on underwater acoustics, seismics, and signal processing, and has coauthored a textbook on computational ocean acoustics. His research has focused on underwater acoustic propagation and signal processing, in particular on the interaction of sound in the ocean with seismic waves in the ocean bottom and the Arctic ice cover. His work has been of theoretical, numerical, and experimental nature.

Prof. Schmidt is a Fellow of the Acoustical Society of America (ASA). He served as Chairman of the ASA Technical Committee on Underwater Acoustics, from 1991 to 1994 and he is currently an Elected Member of the Executive Council of ASA. He is the 2005 Recipient of the ASA Pioneer of Underwater Acoustics medal.